

## CHAPTER 95

### DISTRIBUTION OF SAND TRANSPORT RATE ACROSS A SURF ZONE

Toru Sawaragi

Professor of Civil Engineering  
Osaka University, Osaka, Japan

and

Ichiro Deguchi

Research Associate of Civil Engineering  
Osaka University, Osaka, Japan

#### ABSTRACT

The distributions of longshore and on-offshore sediment transport rates in a surf zone were measured by an apparatus which was able to separately record both components of the sediment transport rate. The characteristics of their distributions were discussed from the bottom shear stresses which were measured by the shear meter under the same wave conditions as the laboratory experiment of the sediment transport.

The maximum bottom shear stress took place at the depth between the breaking depth of waves and the depth where the velocity of the longshore current showed a maximum. On the other hand, the maximum on-offshore and longshore sediment transport rates occurred at the depth slightly shallower than the depth where the maximum bottom shear stress took place. What's more, the longshore sediment transport rates were represented by the longshore current velocity and the bottom shear stress generated by waves and the longshore current. However, the distribution of the on-offshore sediment transport rates showed more complicated profile than that of the longshore sediment transport rates because there were no eminent unidirectional flow in the direction normal to the shore line. Therefore, the on-offshore sediment transport rates could not be formulated by the bottom shear stresses.

#### 1. Introduction

In the problems of the coastal sediment, the sediment transport is usually considered to be divided into the longshore and the on-offshore components for convenience. The longshore sediment transport rate has been investigated from an energy principle approach, and the on-offshore sediment transport has been investigated in the process of equilibrium beach profiles. However, the sediment in the surf zone do not move in the directions normal and parallel to the shore line independently. Although some investigations concerning the distribution of the longshore sediment transport rate in the surf zone based on both energy and force principle approach have been proposed (Thornton(1972)

and Komar(1977)), those theories have not been verified thoroughly by fields or model beach experiments because of the lack of information about wave deformations and wave-induced flow conditions, and the difficulty of the measurement of the longshore sediment transport rate in the surf zone.

The authors devised an apparatus which was able to separately record the longshore and the on-offshore sediment transport rates, the distributions of each component of the sediment transport rate along a line normal to the shore line across the surf zone were measured by using this apparatus in a field as well as in a laboratory model beach. Furthermore, the distribution of bottom shear stresses, which directly cause sediment movements on a sea bottom, along a line normal to the shore line was also measured by a shear meter on a fixed bed in a laboratory under the same wave conditions as the laboratory experiment of sediment transport rates.

The characteristics of a bed load caused by waves and wave-induced longshore current were discussed with respect to the distribution of the bottom shear stress and the formula on the rate of longshore sediment transport was proposed.

## 2. Equipments and procedures to measure the sediment transport rate.

In the surf zone where the wave-induced longshore current occurs, sediment particles at the bottom are moved by the water-particle-motion combined waves and the longshore current. As a results, the directions of sediment movements change with time according to the phase of the wave motion or the relative velocity of the water particle due to waves to the velocity of currents. The authors devised the method to analyze the longshore and the on-offshore sediment transport rates by measuring the sediment volume which are moved by uprush and downrush separately, by using a sand trap as shown in Fig.1. During the measurement, this sand trap was buried in the sea bottom till the upper part of the trap and its surrounding sea bottom were on the same level. Pebble stones were also put around the trap to prevent local scouring due to waves in the field. In Fig.1, the following symbols are used:

$a$  : the diameter of the sand trap

$|\vec{q}_u|$  and  $|\vec{q}_d|$ : the sediment transport rates per unit length per unit time when sediment are moved by uprush and downrush,

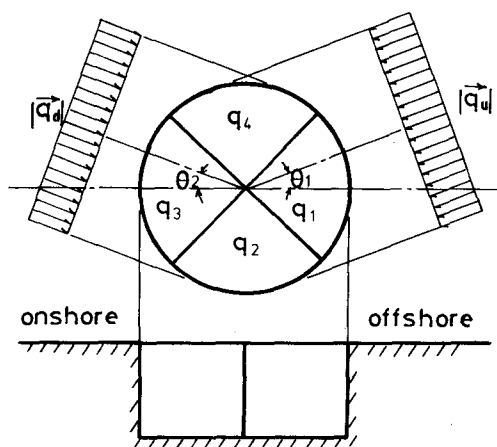


Fig.1 Sand trap

respectively.

$\theta_1$  and  $\theta_2$ : the angles between a line normal to the shore line and the directions of the sediment movement (the clockwise position being positive), respectively.

where  $q_{u1}$  and  $q_{d1}$  are defined by assuming the following model of the sediment transport:

a) When the sediment moves toward the shore line, the volume of the sediment which can be transported by any current per unit area at the bottom is  $q_{u1}^*$  and the velocity of the sediment transport is  $|\vec{u}_{s1}|$ , the direction of which makes an angle  $\theta_1$  with the normal to the shore line. Hence the sediment transport rate per unit length per unit time when the sediment is moved by uprush equals  $|\vec{q}_{u1}| = q_{u1}^* \cdot |\vec{u}_{s1}|$  and the longshore and the on-offshore components of the velocity of the sediment transport equal  $|\vec{u}_{s1}| \sin \theta_1$  and  $|\vec{u}_{s1}| \cos \theta_1$ , respectively.

b) When the sediment is moved toward offshore by downrush, the volume of the sediment which can be transported is  $q_{d1}^*$  and the velocity of the sediment transport is  $|\vec{u}_{s1}|$ , the direction of which makes an angle  $\theta_2$  with the normal to the shore line. Here, the sediment transport rate when the sediment is moved by downrush equals  $|\vec{q}_{d1}| = q_{d1}^* \cdot |\vec{u}_{s1}|$  and the longshore and the on-offshore components of the velocity of the sediment transport equal  $|\vec{u}_{s1}| \sin \theta_2$  and  $|\vec{u}_{s1}| \cos \theta_2$ , respectively.

Based on these assumptions, the longshore and the on-offshore sediment transport rates per unit length per unit time,  $q_x$  and  $q_y$ , are given as follows:

$$\begin{aligned} q_x &= q_{u1}^* |\vec{u}_{s1}| \sin \theta_1 - q_{d1}^* |\vec{u}_{s1}| \sin \theta_2 = |\vec{q}_{u1}| \sin \theta_1 - |\vec{q}_{d1}| \sin \theta_2 \\ q_y &= q_{u1}^* |\vec{u}_{s1}| \cos \theta_1 - q_{d1}^* |\vec{u}_{s1}| \cos \theta_2 = |\vec{q}_{u1}| \cos \theta_1 - |\vec{q}_{d1}| \cos \theta_2 \end{aligned} \quad (1)$$

In these equations,  $|\vec{q}_{u1}|$ ,  $|\vec{q}_{d1}|$  and  $\theta_1$ ,  $\theta_2$  can be calculated volumetrically from the sediment which were trapped in the individual compartments of the sand trap by using the following relations:

For  $0 < \theta_1, \theta_2 < \pi/4$

$$\begin{aligned} q_1 &= |\vec{q}_{u1}| \sqrt{2} \cos \theta_1, \quad q_2 = |\vec{q}_{u1}| a (1 - \cos(\theta_1 + \pi/4)) + |\vec{q}_{d1}| a (1 - \cos(\pi/4 - \theta_2)) \\ q_3 &= |\vec{q}_{d1}| \sqrt{2} \cos \theta_2, \quad q_4 = |\vec{q}_{d1}| a (1 - \cos(\theta_2 + \pi/4)) + |\vec{q}_{u1}| a (1 - \cos(\pi/4 - \theta_1)) \end{aligned} \quad (2)$$

For other values of  $\theta_1$  and  $\theta_2$ , similar relations as eq. (2) are used to calculate  $|\vec{q}_{u1}|$ ,  $|\vec{q}_{d1}|$  and  $\theta_1$ ,  $\theta_2$  except when  $-\pi/2 < \theta_1 < -\pi/4$ ,  $\pi/4 < \theta_2 < \pi/2$  and  $\pi/4 < \theta_1 < \pi/2$ ,  $-\pi/2 < \theta_2 < -\pi/4$ . In these case, the velocity of the longshore current is greater than the water-particle velocity due to the wave, and the on-offshore sediment transport can be neglected.

### 3. Field measurements of the sediment transport rate in the surf zone.

The authors conducted the measurements with this sand trap in the two natural beaches shown in Fig. 2. Isonoura Beach looks out on the Pacific Ocean and has a straight beach of about 1 km, the slope of which is about 1/80. The median grain size of the beach materials is about 0.2 mm. The incident wave steepnesses are usually flat and wave heights are relatively high. Matsuho Beach is located at the southern end of Awaji Isl. and has a convex beach of about 50 m, the slope of which is about 1/15. The median grain size of the beach materials is about 2.0 mm. The incident wave steepnesses are usually steep and wave heights are

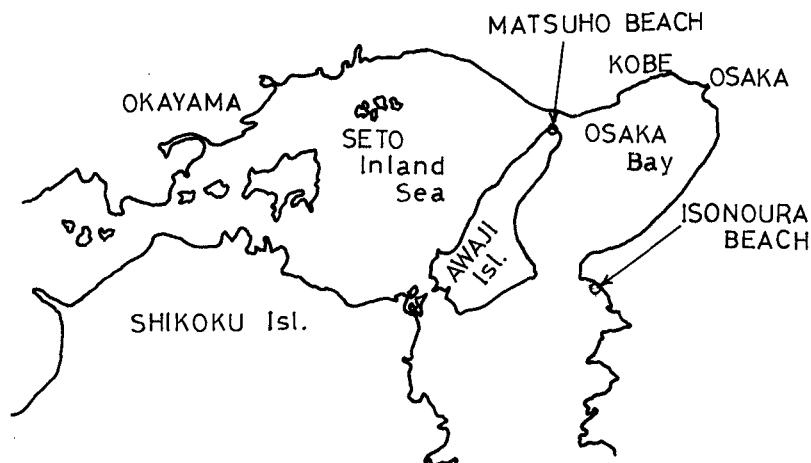


Fig.2 Sites of field measurements of sediment movements.

relatively small. The diameter of the sand trap used in these field experiments was  $50\text{cm}$  and the depth was  $30\text{cm}$ – $40\text{cm}$ . 10 sand traps were buried equi-distance between the wave run-up height and about  $3.0\text{m}$  below the mean water level. The incident wave characteristics were also recorded by the pressure-type wave gauge.

Figs.3 and 4 show examples of the distributions of the longshore and the on-offshore sediment transport rates along beach profiles measured in these two beaches.

Figs.3(a) and (b) indicate the results obtained at different times in Isonoura Beach. This beach has a large surf zone of about  $100\text{m}$  width because of the gentle slope and flat and high incident wave height. The distribution of the longshore and the on-offshore sediment transport rates shown in Fig.3(a) indicates one peak slightly seaward from the shore line. While the profile of the distribution of the longshore sediment transport rate shown in Fig.3(b) indicates two peaks near the shore line and a location slightly shallower than the breaking depth of the significant incident wave.

Figs.4(a) and (b) indicate the results obtained in Matsuho Beach. Since Matsuho Beach has a steep beach slope which consists of relatively large beach materials, and furthermore, since the incident wave heights are usually small, the length of the surf zone is small (about  $5\text{m}$ ). So, as shown in Fig.4, the longshore and the on-offshore sediment transport were concentrated in a narrow range near the shore line. And the profiles of the distribution of the longshore and the on-offshore sediment transport rates indicated one keen peak which was sometimes above the shore line.

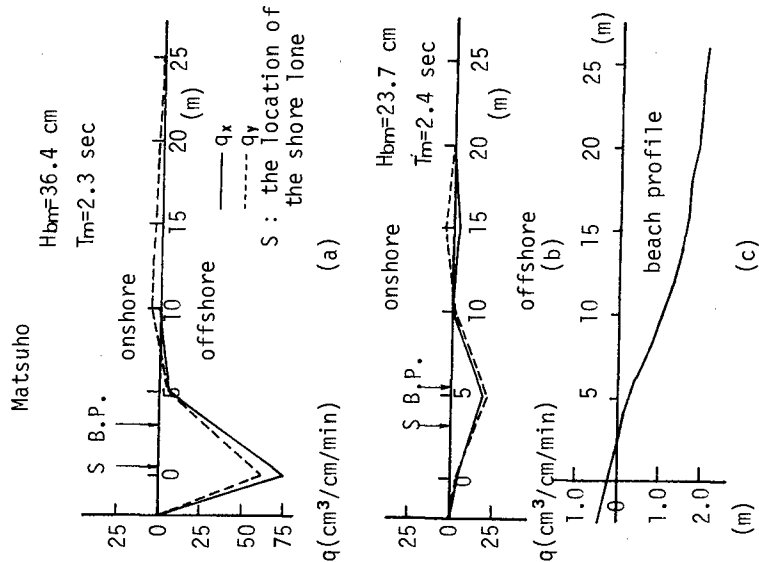


Fig. 4 Distribution of sediment transport rate measured at Matsuho Beach.

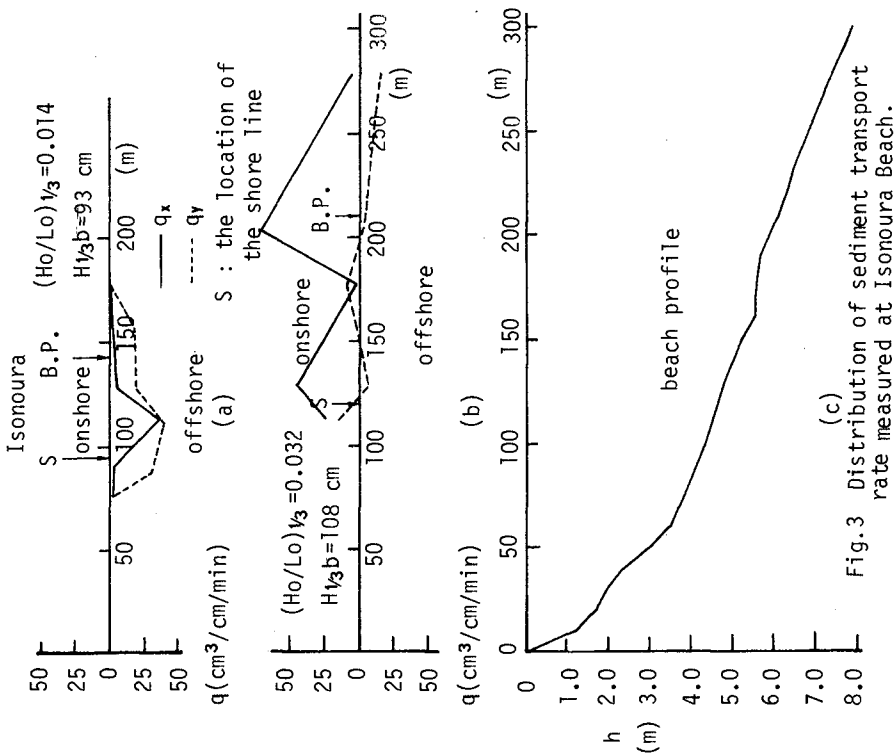


Fig. 3 Distribution of sediment transport rate measured at Isonoura Beach.

#### 4. Measurements of the sediment transport rate and bottom shear stresses on a model beach.

It appears very difficult to find the general characteristics of the sediment transport from the field data as shown in Figs.3 and 4 because of the irregularities of incident waves and the changes of the still water level due to tides. Therefore, the authors conducted measurements of the sediment transport rates in the surf zone on a model beach with a movable bed. In addition, bottom shear stresses which directly cause sediment movements on a fixed bed were measured in order to make more detailed investigation of the mechanism of the sediment transport in the surf zone.

##### 4-1. Measurements of the sediment transport rate on a model beach.

Movable bed experiments were conducted by using a wave basin of 20<sup>m</sup> width, 30<sup>m</sup> length and 0.6<sup>m</sup> depth. At one end of the basin was equipped a straight 12<sup>m</sup> long model beach with a slope of 1/20. At the other end of the basin was installed a flap-type wave generator which generated an incident wave making an angle 30° with the shore line of the model beach at the water depth of 38<sup>cm</sup>. Three kinds of waves of which the steepness in a deep water were about 0.02, 0.04, and 0.06 were propagated. Two kinds of beach materials, median grain size  $d_{50}$  being 0.34<sup>mm</sup> and 0.68<sup>mm</sup>, were used. However, the wave height in deep water was kept constant at about 6<sup>cm</sup>.

Sediment transport rates were measured by 10 sand traps buried between the shore line and at the depth of 10<sup>cm</sup>. The diameter of the sand trap was 10<sup>cm</sup> with a depth of 7<sup>cm</sup>. Wave height distributions in the surf zone were measured by capacitance-type wave gauges, and the longshore current velocity and the wave direction were recorded by 16<sup>mm</sup> high-speed cine camera equipped at a height of 4<sup>m</sup> above the wave basin.

##### 4-2. Equipments and procedures to measure bottom shear stresses.

The bottom shear stress was measured by a shear meter which is shown in Fig.5. In Fig.5, a shear force acting on the shear plate ① is measured by converting the force into a moment of the supporting shaft ②. The shear plate is subjected to a resultant force due to wave pressure gradient force and the shear force. Thus, the shear force is calculated by subtracting pressure gradient force, measured by the pressure tube ③ equipped at both ends of the shear plate, from the resultant force measured by the shear plate.

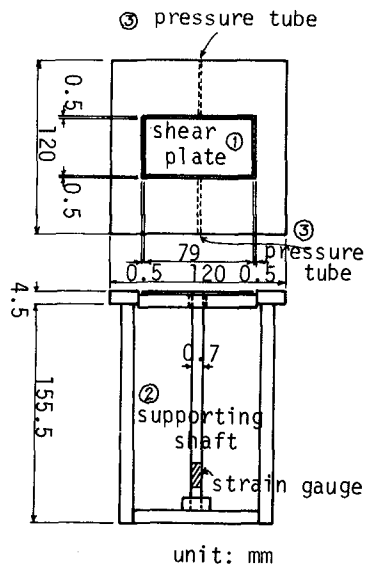


Fig.5 Shear plate

However, in the experiments, the bottom shear stresses were caused by waves and currents and the direction of their respective water-particle-motion made an angle of about  $90^\circ$ . Therefore, it was assumed that the water-particle movements normal to the direction of the shear stress do exist. Then the authors made many concave gratings under the shear plate to prevent these water-particle movements. And the bottom shear stress was measured as the longshore and the on-offshore components separately at about the same point as the measurement of the sediment transport. Hereafter, these components of the bottom shear stress are represented by  $\tau_x$  and  $\tau_y$ , respectively.

## 5. Experimental results.

### 5.1 Distributions of $q_x$ and $q_y$ .

The distributions of averaged  $q_x$  and  $q_y$  measured twice within  $10^{\text{min}}$  after wave propagation in the experiments of  $d_{50} = 0.34^{\text{mm}}$  and  $d_{50} = 0.68^{\text{mm}}$  are shown in Figs.6 and 7, while Fig.8 shows the distributions of the velocity of the longshore current  $U$  and wave height  $H$ . In these Figs.,  $q_{xm}$  and  $q_{ym}$  indicate the maximum value of  $q_x$  and  $q_y$ . And  $U_m$  is the maximum longshore current velocity and  $H_b$  is the breaking wave height.  $Y$  is the distance from the shore line and  $Y_b$  is the distance from the shore line to the breaking point.

When  $d_{50} = 0.68^{\text{mm}}$  ( $H_0/d_{50} = 88$ ) as shown in Figs.6 and 8(a), the maximum  $q_x$  and  $q_y$  occurred at  $Y/Y_b = 0.6$  which was slightly seaward than the point where the velocity of the longshore current showed a maximum value regardless of  $H_0/L_0$ . Besides, the direction of the on-offshore sediment transport was almost offshore. According to the continuous equation for the sediment transport, the distribution of  $q_y$  as shown in Fig.6(b) causes the following modes of beach deformation as erosion in the range of  $Y/Y_b < 0.6$  and accretion in the range of  $Y/Y_b > 0.6$  and these modes of beach deformation were confirmed in our experiments.

On the other hand, in the case of  $d_{50} = 0.34^{\text{mm}}$  in Fig.7(a), maximum  $q_x$  took place at  $Y/Y_b = 0.8$ , which was more toward the seaward side than the former case and the profiles of the distribution showed saddle shapes in the region of  $Y/Y_b < 0.6$ , while the distribution of  $q_y$  shown in Fig.7 (b) indicates complicated figures, maximum  $q_y$  occurring at the same point as  $q_x$ . Furthermore, it can be seen from Fig.7 that a fair amount of sediment transport occurred in the region of  $Y/Y_b > 1.0$ .

### 5-2. Profiles of the distribution of $\tau_{xm}$ and $\tau_{ym}$ .

Fig.9 shows an example of the distribution of measured maximum bottom shear stresses in nondimensional form by dividing by  $\rho g H_b$  along a beach profile together with the distribution of the velocity of the longshore current and the wave heights measured at the same time, where  $\rho$  is the density of the water and  $g$  is the acceleration due to the gravity.

In the region of  $Y/Y_b > 0.8$  in Fig.9, both  $\tau_{xm}/\rho g H_b$  and  $\tau_{ym}/\rho g H_b$  increase monotonously as  $Y/Y_b$  decreases. And in the region of  $Y/Y_b < 0.8$ ,

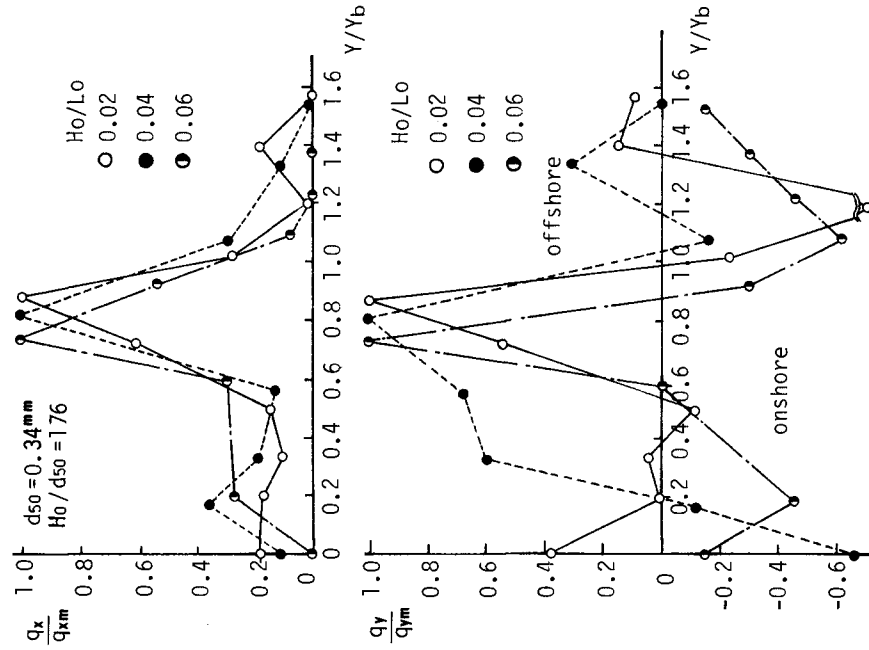


Fig.6 Distribution of sediment transport rate.

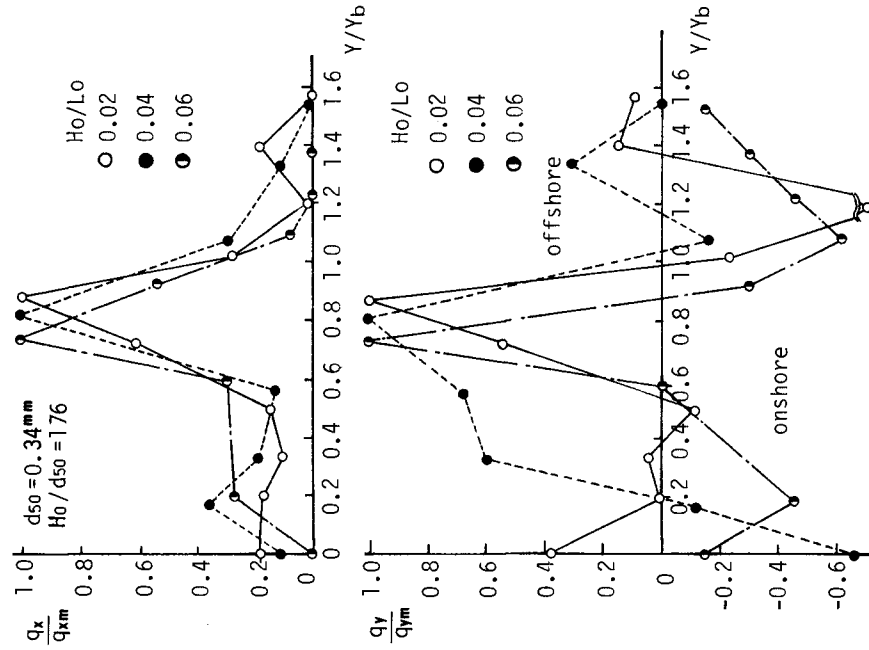


Fig.7 Distribution of sediment transport rate.

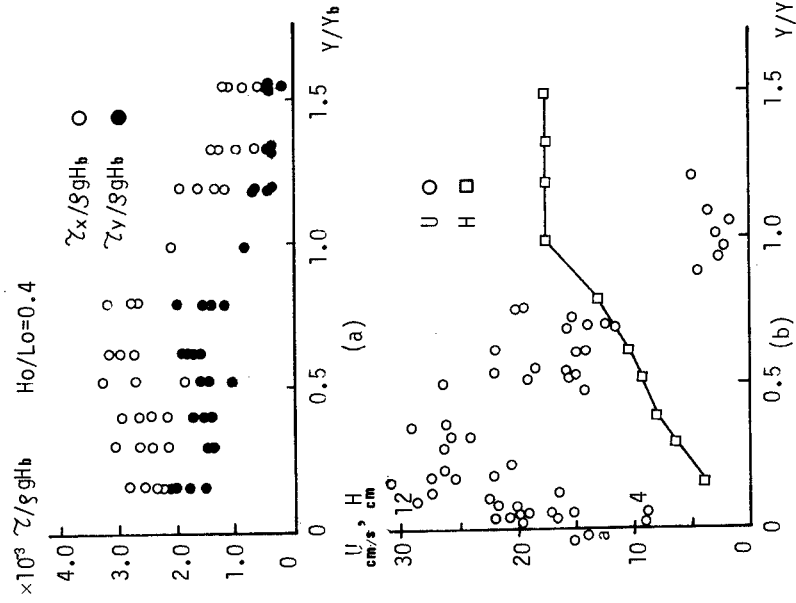


Fig. 9 Distribution of bottom shear stress, longshore current velocity and wave height.

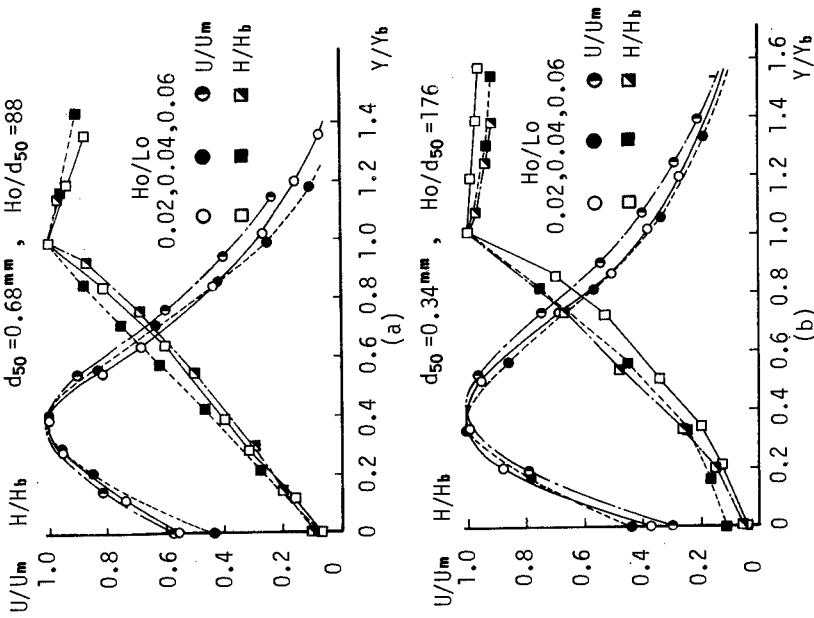


Fig. 8 Distribution of longshore current and wave height.

$\tau_{ym}/\rho g H b$  indicates almost constant values. On the other hand, the distribution of  $\tau_{xm}/\rho g H b$  in this region is minimum at  $Y/Y_b=0.6$  and maximum at  $Y/Y_b=0.3$  where the velocity of the longshore current became significant as shown in Fig.9(b).

Bijker(1966) studied the problem of the bottom shear stress due to a combined wave and current action when they were given independently. In his theory, the bottom boundary layer was mainly determined by a current. So, when his results were applied to our experiments  $\tau_{xm}$  surpasses  $\tau_{ym}$  ( $\tau_{xm}/\tau_{ym}>5$ ) in the whole range of the surf zone. However, because the longshore current is caused by waves, it can be thought reasonably that the boundary layer in the surf zone is determined almost by the wave characteristics and Bijker's theory can not be applied in the surf zone.

Therefore, the authors assume the effects of the longshore current on the bottom shear stress as follows:

Consider the water particle velocity which is composed of the wave and the longshore current just outside the bottom boundary layer as shown in Fig.10. In this figure, the following symbols are used:

$U$  : the velocity of the longshore current.

$u_{bm}$  : the maximum water-particle velocity by waves.

$\theta$  : the angle between the direction of wave propagation and a line normal to the shore line.

$V$  : the composite water-particle velocity of the wave and the longshore current.

$\beta$  : the angle between the direction of the composite bottom shear stress and a line normal to the shore line ( $=\tan^{-1}(\tau_{xm}/\tau_{ym})$ ).

and  $\rightarrow$  indicates a vector. It is now assumed that the maximum bottom shear stress acts in the direction of the vector sum of the longshore current and the maximum water-particle velocity by the wave, which makes an angle  $(\pi/2-\theta_m)$ , and is expressed by the following relation,

$$\tau_m = \rho f |\vec{V}_m|^2$$

$$\text{where } |\vec{V}_m|^2 = (u_{bm} \cos \theta_m)^2 + (u_{bm} \sin \theta_m + U)^2 \quad (3)$$

and  $f$  is the friction factor. In this case, the longshore and the on-off-shore components of  $\tau_m$  become

$$\tau_{xm} = \tau_m (u_{bm} \cos \theta_m) / |\vec{V}_m|$$

$$\tau_{ym} = \tau_m (u_{bm} \sin \theta_m + U) / |\vec{V}_m| \quad (4)$$

and the following relation can be obtained,

$$\frac{\tau_{xm}}{\tau_{ym}} = (\tan \theta_m + \frac{U}{u_{bm}}) \sec \theta_m \quad (5)$$

Now, let  $(\tau_{xm}/\tau_{ym})_0$  be the ratio when there is no current ( $U=0$ ),  $(\tau_{xm}/\tau_{ym})_0 = \tan \theta_m$  from eq.(5), and eq.(5) can be written as

$$\left( \frac{\tau_{xm}}{\tau_{ym}} - \left( \frac{\tau_{xm}}{\tau_{ym}} \right)_0 \right) \cos \theta_m = \frac{U}{u_{bm}} \quad (6)$$

Fig.11 shows the relation of eq.(6) where  $u_{bm}$  was calculated from the relation

$$u_{bm} = \sqrt{g(h+H)} (H/2h) \quad (7)$$

and  $H$  in eq.(7) was obtained from the experimental results.

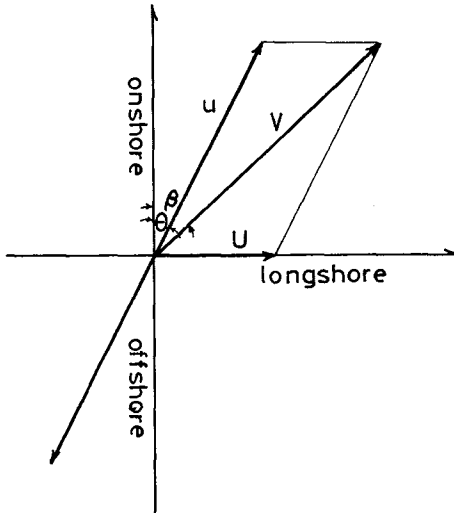


Fig.10 Composite water-particle velocity

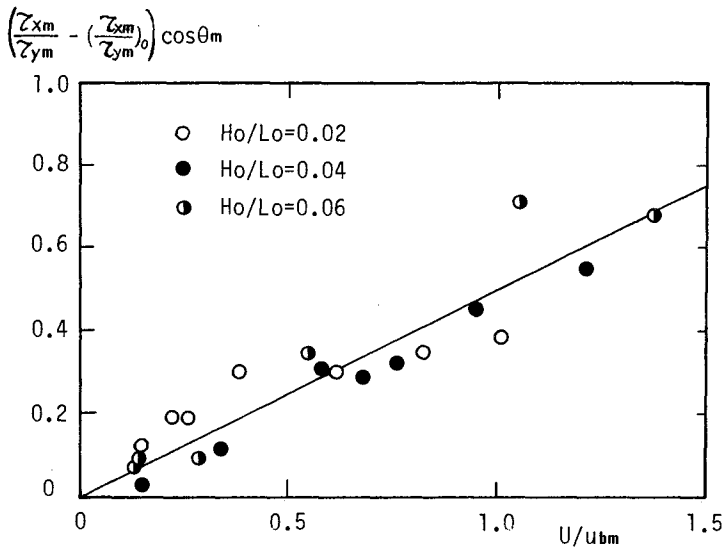


Fig.11 Increase of the longshore component of bottom shear stresses due to longshore current.

It can be seen from Fig.11 that  $(\tau_{xm}/\tau_{ym} - (\tau_{xm}/\tau_{ym})_0)\cos\theta_m$  increase linearly as  $U/u_{bm}$  increase regardless of  $H_0/L_0$ . However, the gradient of the straight line drawn in Fig.11, which indicates the approximate relation between the two quantities of eq.(6), is about 1/2. From this fact, the velocity of the longshore current just outside the boundary layer assumes a value about half of the velocity at the surface and the following expression for  $\tau_{xm}/\tau_{ym}$  and  $\tau_{xm}$  can be obtained,

$$\frac{\tau_{xm}}{\tau_{ym}} = \frac{U}{2u_{bm}\cos\theta_1} + \tan\theta_m \quad (8)$$

$$\tau_{xm} = (\tau_{xm}^2 + \tau_{ym}^2)^{1/2} = \left\{ \left( \frac{U}{2u_{bm}\cos\theta_m} + \tan\theta_m \right)^2 + 1 \right\}^{1/2} \tau_{ym} \quad (9)$$

However, there are some complexities involved calculating these components of the bottom shear stress according to eqs.(3) and (4), and the authors tried to express  $\tau_{ym}$  by using the wave characteristics only as defined by

$$\tau_{ym} = \rho f_y u_{bm}^2 \quad (10)$$

Fig.12 shows the relation between  $f_y$  calculated from eq.(10) and the Reynolds' number  $Ret = u_{bm}^2 T/\nu$ , where  $T$  is the wave period,  $\nu$  is a coefficient of the kinetic viscosity of the water,  $a_s$  is an amplitude of the water-particle movement just outside the boundary layer and  $k_s$  is the equivalent roughness element. The full line in this figure indicates the relation obtained from the laminor theory and the dotted line indicates the limit of the transitional range from laminor to turbulent flow condition obtained by Reidel et.al.(1972). It can be seen from Fig.12 that  $f_y$  calculated from our experiments are a few times larger than those in the laminor boundary layer.

From the results mentioned above, it can be seen that bottom shear stresses can be calculated easily from Fig.12 and eqs.(8),(9) and (10).

### 5-3. Relations between $q_x$ and the bottom shear stress.

As shown in Figs.6.7 and 8, there exists a certain relation between  $q_x$  and the bottom shear stress. Therefore, the authors investigated the distribution of the longshore sediment transport rate along the beach profile, based on the measured results of the bottom shear stress by considering the velocity of the longshore current as a velocity of the sediment transport. However, since the bottom shear stress was measured on a smooth-fixed bottom, there still remains some questional problems as to whether the same bottom shear stress as measured on a fixed bed can be applied to a movable bed or not. According to Kajiura(1968), the flow condition in the bottom boundary layer in the surf zone was laminor or smooth-turbulent when the bottom was flat, and rough-turbulent when sand ripples were formed in a movable bed. However, in the surf zone, large turbulence was brought into the water from the surface by breaking. And it was estimated that the wave energy loss in the surf zone was some hundred times the amount of energy dissipated due to the bottom shear stress(Sawaragi et.al.(1974)). Therefore, the flow condition in the surf zone seems to determined by the intensity of the turbulence by wave breaking regardless of the bottom configurations. Hence, the application of the results in a fixed bed to the movable bed is justified. Figs.8 and 9(b) may verify the above-mentioned consideration to some extent.

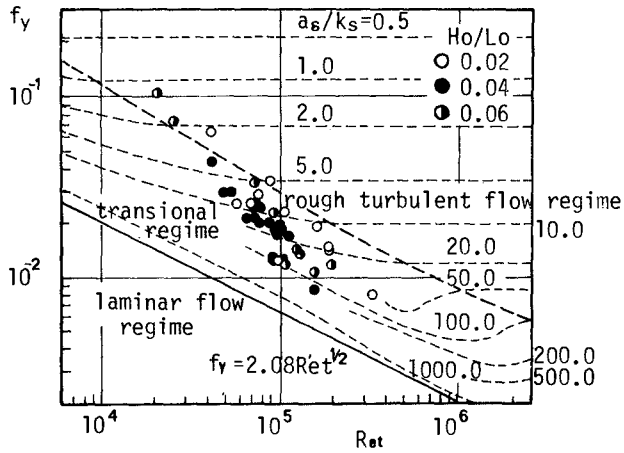


Fig.12 Friction factor calculated from the on-offshore component of the bottom shear stress and water-particle velocity.

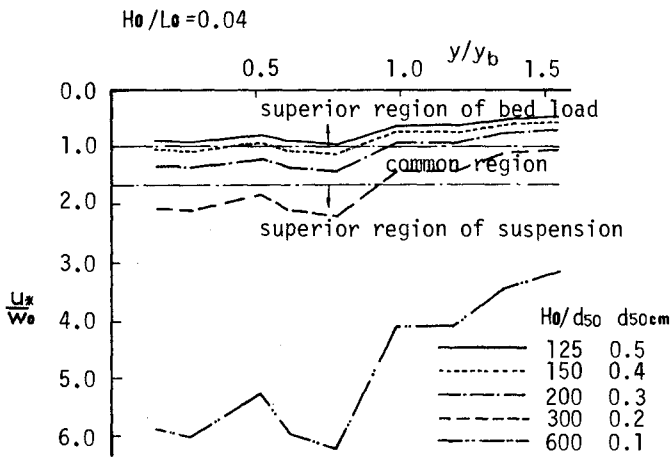


Fig.13 Distribution of  $u_x/W_o$

That is, the conditions of the wave attenuation in the surf zone are similar and there seems to be no significant difference between the distribution profiles of the velocity of the longshore current of various bottom configurations. Therefore, the authors considered that the bottom shear stresses, as measured on the fixed bed, acted with almost the same intensity on the movable bed in the surf zone. Hence the longshore sediment transport rate can be expressed as a function of the bottom shear stress and the velocity of the longshore current.

Based on the above-mentioned way of thinking, the maximum longshore sediment transport takes place at the same location regardless of the size of the beach materials. However, this fact is different from the experimental results in that the location where the maximum longshore sediment transport of  $d_{50} = 0.68^{mm}$  took place was shallower than that of  $d_{50} = 0.34^{mm}$ .

The sand trap shown in Fig.1 was used in our experiment for the purpose of recording the volume of the sediment which were transported as the bed load. In the region where the turbulence at the bottom is strong enough to bring the sediment into suspension from the bed, this kind of sand trap does not function effectively. Therefore, it is worthwhile to clarify the region where both bed materials of  $d_{50} = 0.34^{mm}$  and  $0.68^{mm}$  in the model beach experiments could be suspended in the surf zone.

It has been recognized that the criterion for the start of the suspension is determined by the ratio  $u_* / w_o$  where  $u_*$  is the bottom shear velocity and  $w_o$  is a falling velocity of the sediment and the region where the suspended load surpasses the bed load is also determined by  $u_* / w_o$  in the field of the open channel flow. For example, these limits concerning the suspension are given by Engelund(1965) and Shinohara (1959) as follow:

$$\begin{aligned} u_* / w_o > 1.0 & \dots \text{the start of suspension} \\ u_* / w_o > 1.7 & \dots \text{suspended load surpasses bed load} \end{aligned} \quad (11)$$

Fig.13 shows  $u_* / w_o$  against  $Y/Y_b$  calculated from the bottom shear stresses measured on a fixed bed and Rubey's formula for  $w_o$  with the parameter  $d_{50}$  and  $H_o/d_{50}$ . As can be seen from Fig.9, measured bottom shear stresses were scattered,  $u_*$  were calculated by using the averaged values of  $\tau_{2m}$  and  $\tau_{3m}$  at the same  $Y/Y_b$  from the relation

$$u_*^2 = \tau_m / \rho = (\tau_{2m}^2 + \tau_{3m}^2)^{1/2} / \rho$$

The criterions given by eq.(11) are indicated in Fig.13 by the dotted and the chain lines. According to these criterions, it is clear that when  $H_o/d_{50} < 125$  ( $d_{50} > 0.5^{mm}$ ), no suspension of the sediment can occur in the whole range of the surf zone, while in the case of  $H_o/d_{50} > 200$  ( $d < 0.3^{mm}$ ) the sediment is suspended in the surf zone and in the case of  $H_o/d_{50} > 300$  ( $d_{50} < 0.2^{mm}$ ), the volume of the sediment transported in suspension is larger than the volume of the sediment transported as bed load at the phase of the maximum bottom shear stress taking place. From these considerations, it can be assumed that in our experiments of the measurements of the sediment transport rates, sediment were transported almost as the bed load. However, a certain amount of the sediment

particles, which can not be predicted by the informations the authors have, were suspended in the region of  $Y/V_b < 0.8$  in the case of  $d_{50} = 0.34^{mm}$ .

Taking account the above-mentioned considerations about the sediment transport, the authors tried to obtain the relationship between nondimensional longshore sediment transport rates  $q_x/Ud_{50}$  and nondimensional force of the sediment transport,  $F = (u_*^2 - u_{*c}^2) / (\rho/\rho_s - 1)gd_{50}$ , as shown in Fig.14, where  $u_*$  is given by eq.(12),  $\rho_s$  is the density of the sediment particle and  $u_{*c}$  is given by Iwagaki(1956) as follows:

$$\begin{aligned}
 u_{*c}^2 &= 80.9d_{50}, & \text{for } d_{50} > 0.303^{cm} \\
 &= 134.6d_{50}^{3/4}, & \text{for } 0.303^{cm} > d_{50} > 0.118^{cm} \\
 &= 55.0d_{50}, & \text{for } 0.118^{cm} > d_{50} > 0.0565^{cm} \\
 &= 8.41d_{50}^{1/2}, & \text{for } 0.0565^{cm} > d_{50} > 0.0065^{cm} \\
 &= 226d_{50}, & \text{for } 0.0065^{cm} > d_{50}
 \end{aligned}
 \tag{13}$$

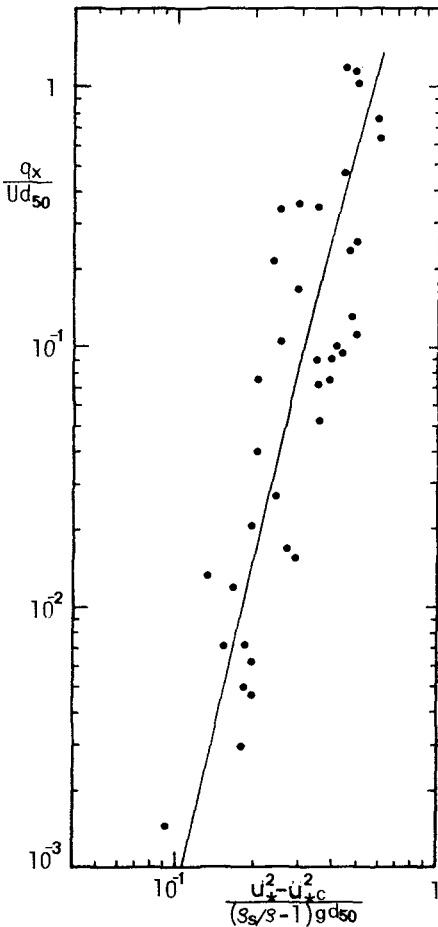


Fig.14 Relation between non-dimensional longshore sediment transport rate and nondimensional force of sediment transport.

Although the data shown in Fig.14 are somewhat scattered, they can be approximately represented by the following two straight lines:

$$\begin{aligned} \frac{q_x}{U_{d50}} &= 86F^{3.7}, \quad \text{for } F \geq 0.3 \\ &= 23F^{4.5}, \quad \text{for } F < 0.3 \end{aligned} \quad (14)$$

In eq.(14),  $u_*$  in  $F$  can be predicted by eqs.(9) and (10). Therefore, the distribution of  $q_x$  can be calculated if the velocity of the longshore current is given.

The predicted distribution of  $q_x$  calculated from eq.(14) are compared with the measured distribution of  $q_x$  in the case of  $H_o/L_o=0.04$  in Fig.15. Here, the longshore current velocity was calculated by the theory of Longuet-Higgins(1970). The parameter  $p$  defined by Longuet-Higgins in his theory was fixed at 0.4 based on the consideration that the location where the longshore current shows the maximum is at about  $Y/Y_b=0.4$  as shown in Fig.9(b). In Fig.15, the predicted  $q_x$  is indicated as a non-dimensional quantity by dividing by the predicted maximum value. From Fig.15, it is found that the distribution of the measured  $q_x$  in the case of  $d_{50}=0.68^{mm}$  where any suspension did not occur in the entire region of the surf zone coincides fairly well with the distribution predicted by eq.(14) and the longshore current velocity presented by Longuet-Higgins. However, the distribution of  $q_x$  in the case of  $d_{50}=0.38^{mm}$  differs from the predicted distribution in the profile. In such conditions of the sediment transport as in the case of  $d_{50}=0.38^{mm}$ , a certain amount of sediment was brought into suspension in the surf zone and it seems necessary to clarify the mechanism of suspension of the bed materials in the surf zone and take account of the quantity of the sediment in suspension in eq.(14)

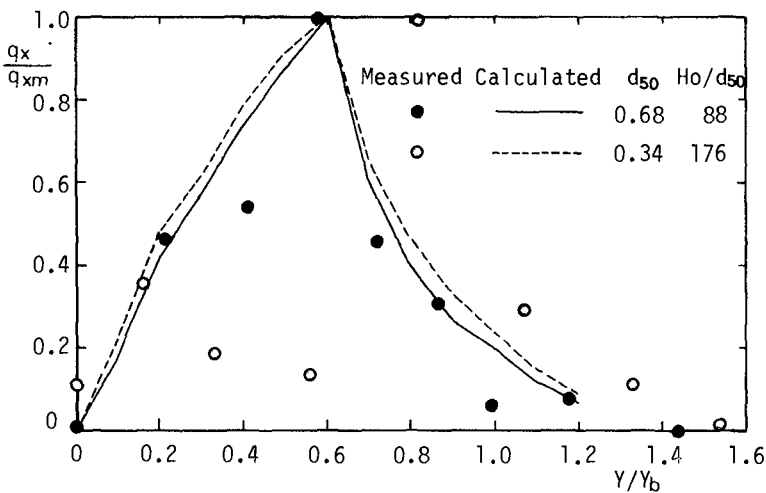


Fig.15 Comparison of the predicted and the measured longshore sediment transport rate.

## 6. Conclusion

The method to separately record the longshore and the on-offshore sediment transport rates, as the bed load, in the surf zone is developed, and the characteristics of the sediment transport in the surf zone are discussed from the bottom shear stresses measured on a fixed model beach.

The following conclusions are drawn from the foregoing study:

1. The distribution of the longshore sediment transport rate as the bed load shows a steep profile compared with the distribution of the longshore current and the maximum longshore sediment transport occurs at the place between the breaking point of incident waves and the location where the velocity of the longshore current shows the maximum value.

2. The maximum on-offshore sediment transport takes place at about the same place as the longshore sediment transport. However, the distribution of the on-offshore sediment transport rate shows more complicated profiles than that of the longshore sediment transport rate; the direction of the on-offshore sediment transport at any location changes with wave characteristics and beach slope from offshore direction to onshore direction.

3. The locations where the maximum longshore and on-offshore sediment transport take place are mainly controlled by the sediment size relative to the wave height.

4. The longshore current has less influence on the on-offshore component of the bottom shear stress than the longshore component, and within the range of the measurements where the wave directions at the breaking points are less than  $20^\circ$ , the on-offshore component of the bottom shear stress is greater than the longshore component of the bottom shear stress. This result differs from the result obtained by Bijker under the condition where waves and currents are given independently. However, the magnitude of the longshore component of the bottom shear stress is not so small as assumed by many investigators in the theory of the longshore current.

5. The longshore sediment transport rate when there are no suspended sediment can be represented by the function of the maximum bottom shear stress and the velocity of the longshore current. However, the estimation of the on-offshore sediment transport rate can not be represented by the maximum bottom shear stress. Further, there still remain some problems with regards estimating the on-offshore sediment transport rate and suspended load quantitatively.

## References

- Thornton, E.B. (1972) : Distribution of sediment transport across the surf zone. Proc. 13th conf. Coastal Eng., pp.1049~1068.
- Komar, P.D. (1977) : Beach sand transport: Distribution and total drift. Proc. ASCE. Vol.103, No.WW2, pp.225~239.
- Bijker, E.W. (1966) : The increase of bed shear in a current due to wave motion. Proc. 10th conf. Coastal Eng., pp.746~765.
- Riedel, H.P., Kamphuis, J.W. and Brebner, A. (1972) : Measurement of bed shear stress under waves. Proc. 13th conf. Coastal Eng., pp.587~604.
- Kajiura, K. (1968) : A model of the bottom boundary layer in water wave. Bull. Earthquake Research Institute, Tokyo Univ., Vol.46, pp.75~123.
- Sawaragi, T. and K. Iwata (1974) : On wave deformation after breaking. Proc. 14th conf Coastal Eng., pp.481~479.
- Engelund, F. (1965) : Turbulent energy and suspended load. Basic Research Progress Report, Technical Univ. of Denmark, No.10.
- Shinohara, K and T. Tsubaki (1959) : On the characteristics of sand waves of the open channels and rivers. Reports of Research Institute for Applied Mechanics, Kyushu Univ., Vol.7, No.25, pp.15~45.
- Iwagaki, Y. (1956) : Basic study on the critical shear velocity for sediment movement in the open channels. Proc. JSCE. Vol.41. (in Japanese)
- Longuet-Higgins, M.S. (1970) : Longshore current generated by obliquely incident sea waves, 1. Journal of Geophysical Research. Vol.75, No.33, pp.6778~6789.